Single-Molecule Kinetics Show DNA Pyrimidine Content Strongly Affects RNA:DNA and TNA:DNA Heteroduplex Dissociation Rates

Hershel H. Lackey[†], Zhe Chen[†], Joel M. Harris[†], Eric M. Peterson^{†*} and Jennifer M. Heemstra^{†,‡,*}

emp@chem.utah.edu 801-581-7938 and jen.heemstra@emory.edu 404-727-7766

Abstract

The heteroduplex hybridization thermodynamics of DNA with either RNA or TNA are greatly affected by DNA pyrimidine content, where increased DNA pyrimidine content leads to significantly increased duplex stability. Little is known however, about the effect that purine or pyrimidine content has on the hybridization kinetics of these duplexes. In this work, single-molecule imaging is used to measure the hybridization kinetics of oligonucleotides having varying DNA pyrimidine content with complementary DNA, RNA, and TNA sequences. Results suggest that the change in duplex stability from DNA pyrimidine content (corresponding to purine content in the complementary TNA or RNA) is primarily due to changes in the dissociation rate, and not single-strand ordering or other structural changes that increase the association rate. Decreases in heteroduplex hybridization rates with pyrimidine content are similar for RNA and TNA, indicating that TNA behaves as a kinetic analog for RNA.

Keywords: TNA, Heteroduplex, Hybridization kinetics, Single-molecule, Purine, Pyrimidine

Nucleic acid molecular recognition plays a central role in biological processes and has been harnessed to control cellular function in synthetic biological systems and enable new biotechnology applications. The most common motif utilized by nucleic acids is that of Watson-Crick-Franklin duplex formation, and this can be categorized by homoduplexes comprised of two nucleic acids having the same backbone structure or heteroduplexes having different backbone structures. While storage of genetic information in Nature primarily relies on DNA:DNA homoduplexes, heteroduplex association and dissociation is a fundamental aspect of many natural and synthetic biological processes. For example, in natural systems RNA:DNA duplexes are associated with DNA replication (through Okazaki fragments), ¹ CRISPR-CAS gene editing,² and telomere reverse transcriptase.³ Alternatively, artificial nucleic acid systems, termed xeno nucleic acids (XNAs) rely on heteroduplex formation during transcription and reverse transcription, which enables in vitro selection of aptamers and nucleic acid enzymes.⁴⁻⁷ Of particular interest among XNA structures is threose nucleic acid (TNA), which utilizes a 2'-3' backbone connection yet retains the ability to base pair with complementary DNA and RNA sequences. TNA benefits from exceptional nuclease stability, imparting utility in synthetic biology and nanotechnology applications that require stability in blood serum or other biological media. Natural and artificial heteroduplexes are also formed in many siRNA and antisense methods, ¹⁰ in addition to imaging techniques such as FISH assays. ¹¹ Finally, the dynamics of heteroduplex formation and information transfer from one nucleic acid variant to another is fundamental in the study of the evolution of nucleic acids and the role they might have played in the origins of life. 12

[†] Department of Chemistry, University of Utah, Salt Lake City, UT, 84112, USA

[‡] Department of Chemistry, Emory University, Atlanta, GA, 30322, USA

^{*}Please address correspondence to Dr. Eric Peterson and Dr. Jennifer Heemstra:

Compared to DNA:DNA or RNA:RNA homoduplexes, far less thermodynamic and kinetic information is available for heteroduplex formation. Heteroduplexes are more challenging to model because the composition of bases on each of the two backbones can greatly influence the conformation and thermodynamics of the duplex. For instance, an RNA:DNA duplex can display significantly different stability and conformational properties than a DNA:RNA duplex having the same base-pairing interactions but with the identity of the bases in each strand swapped. Specifically, thermodynamic and conformational studies on RNA:DNA and TNA:DNA duplexes have shown that increased purine content on the RNA or TNA sequence generally increases the stability of the duplex. However, little is known about how the purine content affects the hybridization kinetics of either of these duplexes. The kinetic parameters illuminate how base content affects the duplex transition state and single-strand conformations, and influence applications such as oligonucleotide therapeutics, where long-lived complexes allow time for nuclease attack, and DNA nanotechnology, where hybridization kinetics affect the rate and mechanism for assembly of nanostructures or circuits.

Single-molecule imaging has proven to be a powerful tool for quantifying the association and dissociation kinetics of oligonucleotide duplexes, as this method allows for direct measurement of hybridization kinetics on a molecule-by-molecule basis 17, 18 and has a number of advantages over ensemble techniques.¹⁹ To initiate a kinetic relaxation response, ensemble kinetics measurements require a perturbation, such as a concentration step, that can affect the observed kinetics due to slow mass transport or mixing. Single molecule techniques can measure kinetics at equilibrium where there are no concentration gradients and mass transport limitations. Additionally, unlike ensemble techniques, single-molecule kinetics measurements provide independent measurements of association and dissociation rates and do not require modeling of transport to interpret kinetic relaxation responses. Finally, by measuring association and dissociation rates at individual molecules, we can better assess heterogeneity, and use that information to correct for nonspecific adsorption or other spurious interactions. ¹⁸ Our lab and others have recently reported methods that use total internal reflection fluorescent TIRF microscopy to image individual fluorescently-labeled DNA hybridizing with DNA immobilized in random arrays on surfaces. 20-22 Videos are acquired of this stochastic hybridization process proceeding at equilibrium, then the centroid coordinate of each fluorescence spot is determined for every molecular event, similar to the imaging techniques used in DNA-PAINT.²³⁻²⁵ By identifying the coordinates of every molecular visit on the surface, the location of DNA probe molecules can be determined by finding clusters of repeated visits to the same location over the course of the video. Once the sites are identified, duplex association and dissociation rates are determined by counting how many frames it takes for a molecule to associate with or dissociate from a site.

In this work, we apply this single-molecule imaging and analysis technique to determine the effect of purine/pyrimidine content on the kinetics of heteroduplex formation. We observe increasing purine content in the RNA or TNA sequences decreases the dissociation rate, while the association rate is slightly reduced. Additionally, we observe similar effects for both RNA and TNA, suggesting that this change in dissociation kinetics arises from the structural adaptation of DNA to these binding partners. These trends in heteroduplex stability are seen in all target sequences studied, and do not appear to be an artifact of dye-labeling or surface immobilization. Together, these data provide new insight into the source of the purine-dependent increase in duplex stability observed for DNA:RNA and DNA:TNA duplexes, and may inform the design of synthetic biology systems where the desired activity would depend on heteroduplex dissociation kinetics.

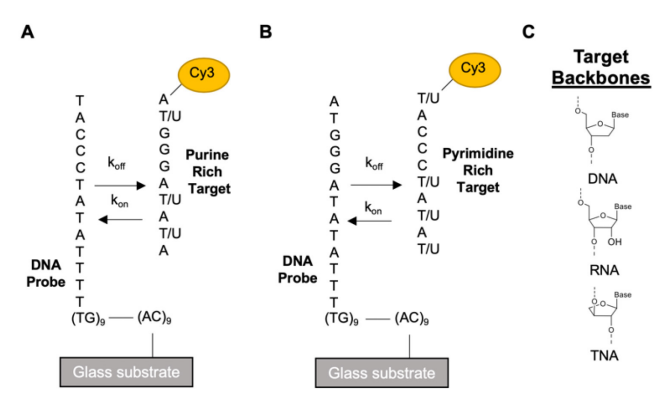


Figure 1. Schematic of the hybridization of fluorescently labeled (A) purine-rich target oligonucleotide or (B) pyrimidine-rich oligonucleotide target with an immobilized complementary DNA probe. (C) Chemical structures of the target oligonucleotides investigated in this study.

To analyze the kinetics of heteroduplex association and dissociation, two different 10 base pair DNA probe sequences were prepared having different recognition regions containing either 30% or 70% purine content; we also synthesized the complementary DNA, RNA, and TNA targets having a Cy3 fluorophore for use in the single-molecule imaging (Figure 1 and Supporting Information). We also prepared additional 9 bp DNA and RNA probes and complementary DNA and RNA targets to test how sequence, surface immobilization, and terminal nucleotide Cy3 attachment affects the kinetics. These target sequences have

66% and 33% purine/pyrimidine content, and have more G-C content (44%), but have no repeated nucleotides as seen in the 10-mer target (see Supporting Information). The DNA probe oligonucleotide includes a 5' repeating (GpT)₉ segment to allow hybridization with a complementary (ApC)₉ 'capture' strand covalently immobilized on a passivated glass slide. The probe oligonucleotide is immobilized at the interface by allowing it to spontaneously hybridize with the capture strand, as described in the Supporting Information.²² The glass slides were fitted to a custom flow cell and mounted on an objective-type TIRF microscope with a variable temperature controller set to 25.0 +/- 0.1 °C. Solutions of probe oligonucleotides were injected into the flow cell and allowed to equilibrate with the surfaceimmobilized DNA before video acquisition. Each DNA probe sequence on the surface was identified by observation of three or more association events within an 80-nm radius, where the microscope-stage drift was corrected using a previously described algorithm.²² The lifetimes of every association and dissociation event were measured at each molecule site. The sites were then filtered to remove those that displayed anomalous kinetics, including excessive single-frame events, hybridization during a only a small portion of the video, and outlier rate constants. The association and dissociation lifetimes were pooled for all filtered probe-site events and plotted as survival-time histograms. These histograms were fit to a single exponential decay function to extract the average association or dissociation time, τ_{on} or $\tau_{\text{off.}}^{22}$ Video exposure times and intervals between exposures were optimized to reduce photobleaching of Cy3 while providing sufficient time resolution to sample the lifetimes of the hybridized duplex. The purine-rich RNA target showed the greatest (30%) influence of photobleaching on the apparent off-rate. For these data, the dependence of the apparent dissociation rate constant on illumination intensity was extrapolated to zero laser power to report k_{off} .

The average τ_{on} and τ_{off} were measured at four different concentrations for each duplex. The association rate constant, k_{on} , was determined by plotting the association rate, $1/\tau_{on}$, vs concentration of target in solution and fitting the curve to Equation 1 (Figure 2 top panels):

$$\frac{1}{\tau_{on}} = k_{on} \cdot [Target] \tag{1}$$

The dissociation rate constant is inversely proportional to τ_{off} (Equation 2):

$$k_{off} = \frac{1}{\tau_{off}} \tag{2}$$

The resulting plots show that $1/\tau_{on}$ varies linearly with concentration of target, indicating minimal unwanted interaction between target molecules in solution at these nM concentrations and that hybridization is not influenced by variations in the structure of the target. The dissociation rate of the 10-mer duplex is independent of target concentration (Figure 2 bottom panels) and k_{off} was determined by averaging the rate constant calculated at each concentration point.

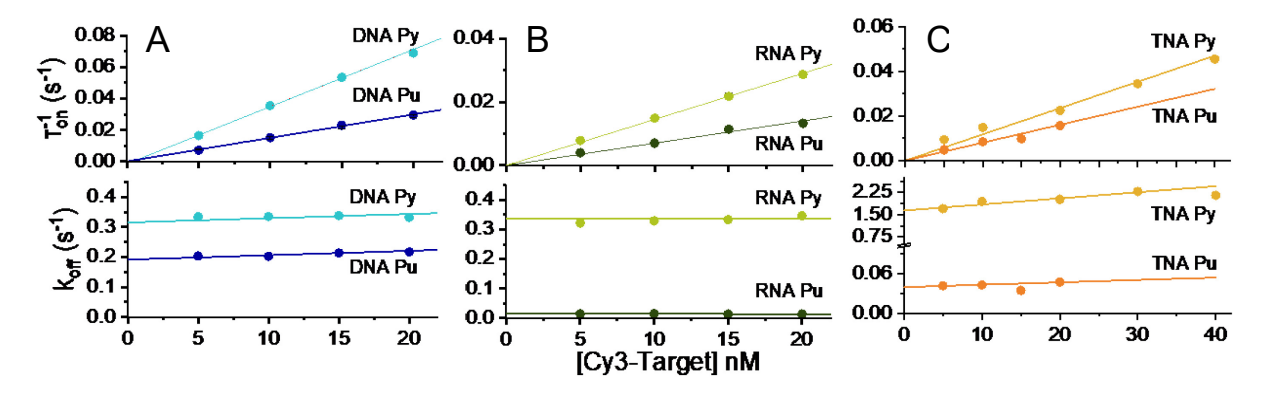


Figure 2. Plot of $1/\tau_{on}$ (top) and k_{off} (bottom) versus [Cy3-probe] for hybridization with A) DNA, B) RNA, and C) TNA 10-mer target sequences. The response of $1/\tau_{on}$ to target concentration was fit to Equation 1 to determine k_{on} . Lines fit to dissociation rates have a slope not significantly greater than zero, showing that dissociation rates are independent of target concentration.

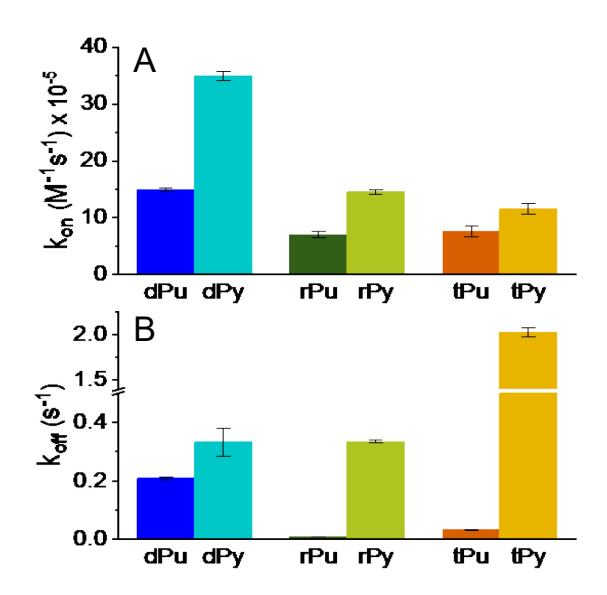


Figure 3. Hybridization kinetics of purine and pyrimidinerich 10-mer DNA:DNA duplexes (dPu and dPy respectively), DNA:RNA (rPu, rPy), and DNA:TNA duplexes (tPu, tPy) with (A) Comparison of k_{on} and (B) comparison of k_{off} . Error bars are two standard deviations of the mean.

The determination of k_{on} and k_{off} for both pyrimidine-rich and purine-rich sequences in the varying backbone contexts enabled comparison of how these structures affected the hybridization rates. Overall, there was a modest increase of 1.5-2.3 fold in k_{on} for pyrimidine-rich vs purine-rich target oligonucleotides for all backbone types (Figure 3A). This effect appears to be a result of the specific sequence context; the alternate 9-mer target sequence has a 2-fold faster association rate for the purine-rich compared to the pyrimidine-rich sequences (SI Figure S6). Interestingly, the kon of DNA homoduplex is higher than that of the RNA or TNA heteroduplexes for both the 9-mer and 10-mer target sequences. These differences in k_{on} however, were overshadowed by the large differences in k_{off} both between the purine/pyrimidine-rich strands and the different sugar backbones (Figure 3B). The k_{off} for purine-rich TNA and

RNA strands was lower by over a factor of 20 compared to the corresponding pyrimidine-rich targets within each class of backbones. The sugar backbone also greatly affected the dissociation rate for purine-rich targets, with a 22-fold variation between slowest and fastest $k_{\rm off}$ values, and a trend of RNA < TNA < DNA. Interestingly, the trend for pyrimidine-rich targets was partially inverted, where DNA \approx RNA < TNA, with a 6-fold difference between the fastest and the slowest. This large increase in dissociation rate with increased pyrimidine content is not an artifact of this specific sequence; the 9-mer target also shows a 15-fold increase in $k_{\rm off}$ for the pyrimidine-rich sequence.

We next determined the binding affinity (K_a) for each duplex using the relationship $K_a = k_{on}/k_{off}$, and then calculated the Gibbs Free energy of hybridization from $\Delta G = -RTln(K_a)$, and compared these to previously reported trends. In line with our previous observations, the K_a for TNA:DNA and RNA:DNA heteroduplexes increased with higher purine content (Table 1). Anosova²⁶ recently reported a K_a value of 7.43 x 10⁶ M⁻¹ for a 10'mer TNA:DNA having 60% purine content using isothermal calorimetry, and this value falls between the K_a value of 0.57 x 10⁶ M⁻¹ for the 25% purine target and 23 x 10⁶ M⁻¹ for the 75% purine target measured in this study (Table 1). The measured ΔG for the purine-rich and pyrimidine-rich DNA:DNA homoduplexes matched well with nearest-neighbor (NN) parameters:²⁷ (https://bioinf.fisica.ufmg.br/app/comparetm.pl) with less than 5% difference between the calculated and predicted values (Table 1). A recently developed calculator for predicting the rates of hybridization for DNA:DNA duplexes also closely matched our measured k_{on} for the pyrimidine rich DNA target with a predicted value of 5.1 x 10^6 M⁻¹s⁻¹ versus the observed value of 3.5 x 10^6 M⁻¹s⁻¹. The measured ΔG values for the RNA:DNA duplexes are less than those predicted by the model,²⁹ and the predicted change in ΔG due to the purine exchange is -2.2 kcal/mol vs the observed -1.7 kcal/mol. However, this difference between the NN parameters and kinetics measurements for RNA:DNA duplexes is likely attributable to coarser NN parameters and ionic strength corrections for these heteroduplexes compared to DNA:DNA homoduplexes.

Table 1. Thermodynamic parameters for DNA:DNA, DNA:RNA, and DNA:TNA duplex hybridization and comparison to NN models.

Sequence	K _a (mol ⁻¹) x 10 ⁶	ΔG° (kcal/mol)	ΔG° _{NN} (kcal/mol)	ΔΔG° _{pu-py} (kcal/mol)
dPu	7.2±0.2	-9.35±0.02	-9.68	0.23
dPy	11±2	-9.57±0.09	-9.68	
rPu	73±8	-10.72±0.07	-12.21	-1.67
rPy	4.3±0.1	-9.05±0.02	-9.98	
tPu	23±3	-10.05±0.07	-	-2.20
tPy	0.57±0.05	-7.85±0.05	-	

Our findings show that the purine-dependent stability trends observed in heteroduplexes are primarily attributable to changes in $k_{\rm off}$. A recent meta-analysis has also shown $k_{\rm off}$ as being the key factor to influence the stability of DNA:DNA, RNA:DNA, and RNA:RNA duplexes, ³⁰ and suggests that the differences in stability between the different backbone types are driven by changes in the free energy of the duplex relative to the transition state. Our data also indicate that the purine content does more to stabilize the duplex structure than to organize the single-stranded target oligonucleotide into a conformation closer in energy to the transition state. Our observations are also in line with data from

Martin³¹ and Martins³² which show that that dA-rU base pairing has reduced strength compared to rA-dT. The TNA duplexes display a similar trend to the RNA duplexes, with TNA exhibiting a slightly larger difference in $k_{\rm off}$ between the purine-rich and pyrimidine-rich strands. The similar trends likely indicate that changes in TNA:DNA duplex stability are primarily due to changes in duplex structure and stability and not the result of single-strand conformations.

In contrast to these large effects observed for DNA:RNA and DNA:TNA heteroduplexes, the modest difference in stability between the purine-rich and pyrimidine-rich DNA:DNA homoduplexes is primarily due to k_{on} . These differences appear to be sequence specific, as the 10-mer and alternate 9-mer targets show opposite trends in k_{on} with purine content. This may be due to differences in single-strand conformation, since one strand is free to diffuse in solution and the other is tethered to the doublestranded anchor section. The strands could adopt different conformations in the free or tethered state which might affect the accessibility of individual nucleotides to initiate hybridization, or the diffusion coefficient in solution. We have previously measured how hybridization kinetics at the interface compare to hybridization in free solution, and immobilization primarily affects the association rate constant.³³ To ensure that the tethering scheme did not significantly influence the stability trends seen for heteroduplex formation, we tested a flipped target-probe system with immobilized RNA and solution-phase DNA. We synthesized chimera probes containing a DNA poly-GpT segment to immobilize them at surface-attached poly-ApC capture sites, and an RNA target-recognition sequence. The immobilized purine-rich 9-mer RNA was still significantly more stable (~14-fold) than the pyrimidine-rich sequence, which was comparable to the increase in stability seen for the equivalent purine-rich Cy3labeled solution-phase 9-mer RNA (~30-fold, see Figure S7). Thus, the differences in heteroduplex stability observed for solution-phase and immobilized RNA-DNA duplexes is primarily due to differences in association rate constant, as seen for the DNA-DNA duplexes.

It should also be considered that cyanine dyes interact with oligonucleotides in a sequence-dependent manner and previous reports have shown that the identity of the terminal base to which the dye is attached can affect duplex stability. Therefore, it is possible that the Cy3 label stabilizes the purinerich and pyrmidine-rich duplex structures to different degrees since they have different 5' terminal nucleotides. Although both the 10-mer and 9-mer target systems share the same terminal base pairs, they differ in the terminal attachment point: Cy3 is bound to a terminal adenosine for the purine-rich 10-mer target, and a terminal thymidine for the pyrimidine-rich target, and vice versa for the 9-mer targets. Despite the differences in Cy3 terminal base attachment, both the 9-mer and 10-mer RNA-DNA duplexes show similar increases in duplex stability with purine content, indicating that this trend is not an artifact of DNA-dye interactions. Since the same nucleotide sequences were used across all three backbones, this contribution to stabilization does not impact our ability to draw conclusions from comparisons of different sugar backbone identities.

This work reinforces previous observations that increased purine content in RNA and TNA leads to increased hybridization stability with complementary DNA. Using single-molecule experiments to measure hybridization kinetics, we observe that this is driven by decreases in $k_{\rm off}$, which suggests that TNA or RNA purine content plays a larger role in stabilizing duplex formation than pre-ordering of the single-stranded oligonucleotides. If pre-ordering of the conformation of the single-stranded RNA or TNA played a significant role, we would expect large increases in the association rate as a result of increased collisional binding efficiency. The kinetics trends between TNA and RNA were also very similar, demonstrating that TNA is an excellent nuclease-resistant kinetic behavioral analog to RNA. Together,

7

these results provide insight into the kinetic behavior of heteroduplexes that are found in Nature and are widely used in synthetic biology systems, and are anticipated to be of utility in informing the design of sequences for biotechnology applications where hybridization kinetics play a key role.

ASSOCIATED CONTENT

Supporting Information

The Supporting Information is available free of charge on the ACS Publications website at DOI: (insert link). Oligonucleotide sequences; slide preparation; kinetic filtering; example histograms; time-interval optimization; references.

AUTHOR INFORMATION

Corresponding Authors

E-mail: jen.heemstra@emory.edu and emp@chem.utah.edu

ORCID

Joel Harris: 0000-0002-7081-8188

Jennifer Heemstra®: 0000-0002-7691-8526

Hershel Lackey: 0000-0001-9132-5764 Eric Peterson: 0000-0001-6694-589X

Present Address

[®] Department of Chemistry, Emory University, Atlanta, GA, 30322, USA

Notes

The authors declare no competing financial interest.

ACKNOWLEDGEMENTS

This work was supported by the DARPA Folded Non-Natural Polymers with Biological Function (Fold F(x)) Program [N66001-14-2-4054]. Any opinions, findings, and conclusions or recommendations expressed in this publication are those of the authors and do not necessarily reflect the views of the Department of Defense. This work was also supported by the National Science Foundation (DMR 1822262 and CHE 1904885 to J. Heemstra and CHE 1608949 and CHE 1904424 to J. Harris). HHL received funding from the the Air Force Institute of Technology Civilian Institute Program (AFIT CI).

REFERENCES

- 1. Ogawa, T., and Okazaki, T. (1980) Discontinuous DNA Replication, Annu. Rev. Biochem 49, 421-457.
- 2. Sander, J. D., and Joung, J. K. (2014) CRISPR-Cas systems for editing, regulating and targeting genomes, *Nat. Biotechnol.* 32, 347.
- 3. Autexier, C., and Lue, N. F. (2006) The Structure and Function of Telomerase Reverse Transcriptase, *Annu. Rev. Biochem 75*, 493-517.
- 4. Taylor, A. I., Pinheiro, V. B., Smola, M. J., Morgunov, A. S., Peak-Chew, S., Cozens, C., Weeks, K. M., Herdewijn, P., and Holliger, P. (2015) Catalysts from synthetic genetic polymers, *Nature 518*, 427.
- 5. Pinheiro, V. B., and Holliger, P. (2014) Towards XNA nanotechnology: new materials from synthetic genetic polymers, *Trends Biotechnol. 32*, 321-328.
- 6. Rangel, A. E., Chen, Z., Ayele, T. M., and Heemstra, J. M. (2018) In vitro selection of an XNA aptamer capable of small-molecule recognition, *Nucleic Acids Res.* 46, 8057-8068.
- 7. Yu, H., Zhang, S., Dunn, M. R., and Chaput, J. C. (2013) An Efficient and Faithful in Vitro Replication System for Threose Nucleic Acid, *J. Am. Chem. Soc.* 135, 3583-3591.
- 8. Schöning, K.-U., Scholz, P., Guntha, S., Wu, X., Krishnamurthy, R., and Eschenmoser, A. (2000) Chemical Etiology of Nucleic Acid Structure: The α -Threofuranosyl-(3' \rightarrow 2') Oligonucleotide System, *Science 290*, 1347-1351.
- 9. Culbertson, M. C., Temburnikar, K., Sau, S. P., Liao, J.-Y., Bala, S., and Chaput, J. C. (2016) Evaluating TNA stability under simulated physiological conditions, *Bioorg. Med. Chem. Lett.* 10, 2418-2421.
- 10. Shen, X., and Corey, D. R. (2018) Chemistry, mechanism and clinical status of antisense oligonucleotides and duplex RNAs, *Nucleic Acids Res.* 46, 1584-1600.
- 11. Cui, C., Shu, W., and Li, P. (2016) Fluorescence In situ Hybridization: Cell-Based Genetic Diagnostic and Research Applications, *Front. Cell Dev. Biol. 4*, 89.
- 12. Yang, Y.-W., Zhang, S., McCullum, E. O., and Chaput, J. C. (2007) Experimental Evidence That GNA and TNA Were Not Sequential Polymers in the Prebiotic Evolution of RNA, *J. Mol. Evol.* 65, 289-295.
- 13. Shaw, N. N., and Arya, D. P. (2008) Recognition of the unique structure of DNA:RNA hybrids, *Biochimie 90*, 1026-1039.
- 14. Lackey, H. H., Peterson, E. M., Chen, Z., Harris, J. M., and Heemstra, J. M. (2019) Thermostability Trends of TNA:DNA Duplexes Reveal Strong Purine Dependence, *ACS Synth. Biol. 8*, 1144-1152.
- 15. Dupuis, Nicholas F., Holmstrom, Erik D., and Nesbitt, David J. (2013) Single-Molecule Kinetics Reveal Cation-Promoted DNA Duplex Formation Through Ordering of Single-Stranded Helices, *Biophys. J.* 105, 756-766.
- 16. Morihiro, K., Kasahara, Y., and Obika, S. (2017) Biological applications of xeno nucleic acids, *Molecular BioSystems* 13, 235-245.
- 17. Shen, H., Tauzin, L. J., Baiyasi, R., Wang, W., Moringo, N., Shuang, B., and Landes, C. F. (2017) Single Particle Tracking: From Theory to Biophysical Applications, *Chem. Rev.* 117, 7331-7376.
- 18. Johnson-Buck, A., Li, J., Tewari, M., and Walter, N. G. (2019) A guide to nucleic acid detection by single-molecule kinetic fingerprinting, *Methods* 153, 3-12.
- 19. Gooding, J. J., and Gaus, K. (2016) Single-Molecule Sensors: Challenges and Opportunities for Quantitative Analysis, *Angew. Chem. Int. Ed. 55*, 11354-11366.
- 20. Johnson-Buck, A., Su, X., Giraldez, M. D., Zhao, M., Tewari, M., and Walter, N. G. (2015) Kinetic fingerprinting to identify and count single nucleic acids, *Nat. Biotechnol.* 33, 730.
- 21. Su, X., Li, L., Wang, S., Hao, D., Wang, L., and Yu, C. (2017) Single-Molecule Counting of Point Mutations by Transient DNA Binding, *Scientific Reports* 7, 43824.
- 22. Peterson, E. M., and Harris, J. M. (2018) Identification of Individual Immobilized DNA Molecules by Their Hybridization Kinetics Using Single-Molecule Fluorescence Imaging, *Anal. Chem.* 90, 5007-5014.

- 23. Schnitzbauer, J., Strauss, M. T., Schlichthaerle, T., Schueder, F., and Jungmann, R. (2017) Superresolution microscopy with DNA-PAINT, *Nature Protoc.* 12, 1198.
- 24. Chen, J., Bremauntz, A., Kisley, L., Shuang, B., and Landes, C. F. (2013) Super-Resolution mbPAINT for Optical Localization of Single-Stranded DNA, *ACS Appl. Mater. Interfaces 5*, 9338-9343.
- 25. Jungmann, R., Steinhauer, C., Scheible, M., Kuzyk, A., Tinnefeld, P., and Simmel, F. C. (2010) Single-Molecule Kinetics and Super-Resolution Microscopy by Fluorescence Imaging of Transient Binding on DNA Origami, *Nano Lett.* 10, 4756-4761.
- 26. Anosova, I., Kowal, E. A., Sisco, N. J., Sau, S., Liao, J.-y., Bala, S., Rozners, E., Egli, M., Chaput, J. C., and Van Horn, W. D. (2016) Structural Insights into Conformation Differences between DNA/TNA and RNA/TNA Chimeric Duplexes, *ChemBioChem 17*, 1705-1708.
- 27. Weber, G. (2015) Optimization method for obtaining nearest-neighbour DNA entropies and enthalpies directly from melting temperatures, *Bioinformatics 31*, 871-877.
- 28. Zhang, J. X., Fang, J. Z., Duan, W., Wu, L. R., Zhang, A. W., Dalchau, N., Yordanov, B., Petersen, R., Phillips, A., and Zhang, D. Y. (2017) Predicting DNA hybridization kinetics from sequence, *Nature Chem.* 10, 91.
- 29. Basílio Barbosa, V., de Oliveira Martins, E., and Weber, G. (2019) Nearest-neighbour parameters optimized for melting temperature prediction of DNA/RNA hybrids at high and low salt concentrations, *Biophys. Chem. 251*, 106189.
- 30. Rauzan, B., McMichael, E., Cave, R., Sevcik, L. R., Ostrosky, K., Whitman, E., Stegemann, R., Sinclair, A. L., Serra, M. J., and Deckert, A. A. (2013) Kinetics and Thermodynamics of DNA, RNA, and Hybrid Duplex Formation, *Biochemistry 52*, 765-772.
- 31. Martin, F. H., and Tinoco, I., Jr. (1980) DNA-RNA hybrid duplexes containing oligo(dA:rU) sequences are exceptionally unstable and may facilitate termination of transcription, *Nucleic Acids Res. 8*, 2295-2300.
- 32. de Oliveira Martins, E., Basílio Barbosa, V., and Weber, G. (2019) DNA/RNA hybrid mesoscopic model shows strong stability dependence with deoxypyrimidine content and stacking interactions similar to RNA/RNA, *Chem. Phys. Lett.* 715, 14-19.
- 33. Peterson, E. M., Manhart, M. W., and Harris, J. M. (2016) Single-Molecule Fluorescence Imaging of Interfacial DNA Hybridization Kinetics at Selective Capture Surfaces, *Anal. Chem. 88*, 1345-1354.
 34. Spiriti, J., Binder, J. K., Levitus, M., and van der Vaart, A. (2011) Cy3-DNA Stacking Interactions Strongly Depend on the Identity of the Terminal Basepair, *Biophys. J. 100*, 1049-1057.

TOC Graphic

